AIP Journal of Applied Physics

# Dispersion of magnetic plasmon polaritons in perforated trilayer metamaterials

Tao Li, Shu-Ming Wang, Hui Liu, Jia-Qi Li, Fu-Ming Wang, Shi-Ning Zhu, and Xiang Zhang

Citation: Journal of Applied Physics **103**, 023104 (2008); doi: 10.1063/1.2828178
View online: http://dx.doi.org/10.1063/1.2828178
View Table of Contents: http://scitation.aip.org/content/aip/journal/jap/103/2?ver=pdfcov
Published by the AIP Publishing



# Dispersion of magnetic plasmon polaritons in perforated trilayer metamaterials

Tao Li,[a),b)] Shu-Ming Wang, Hui Liu, Jia-Qi Li, Fu-Ming Wang, and Shi-Ning Zhu[a),c)]
*National Laboratory of Solid State Microstructures, Nanjing University, Nanjing 210093, People's Republic of China*

Xiang Zhang
*5130 Etcheverry Hall, Nanoscale Science and Engineering Center, University of California, Berkeley, California 94720-1740, USA*

(Received 30 October 2007; accepted 2 November 2007; published online 22 January 2008)

Multiple magnetic plasmon polariton (MPP) modes were recently explored in a well-known system—metal/insulator/metal layered structure perforated with periodic holes array [Appl. Phys. Lett. **90**, 251112 (2007)]. Now, we consequently study the dispersions of the MPP modes in similar systems with rectangular hole arrays by analyzing the detailed optical transmittances at oblique incidences. Significantly, our results provide a definite polarization-dependent dispersion property of MPP modes: strong dispersive MPP$(\pm 1, \pm 1)$ modes with the degeneration broken up and a remained degenerate MPP$(0, \pm 1)$ mode for *s*-polarization and almost flat dispersions of all MPP modes for *p*-polarization. Such a phenomenon is explained by the different coupling intensities among the artificial "magnetic atoms." This finding helps us to make a deeper understanding on the artificial magnetic excitations in this trilayer metamaterial. © *2008 American Institute of Physics*. [DOI: 10.1063/1.2828178]

## I. INTRODUCTION

Metal/insulator/metal trilayer metamaterial with periodic hole array was invented to achieve negative refraction property in 2005,[1] and was subsequently developed to exhibit improved performance at higher frequencies by structural optimizations.[2–4] The fundamental physics to realize the negative index in this system (or the so-called fishnet structure) is base on the artificial "magnetic atoms" consisted of the magnetically excited *LC*-resonance between the two coupled metallic layer segments and the "electric atoms" from continuous metallic strip parts, which produce simultaneous negative permeability and permittivity accordingly. Such kind magnetic responses, including those from the typical magnetic atom–split resonant ring (SRR),[5] which play the key role in the negative index metamaterial (NIM), were regarded as the localized resonance in a common sense.[6–9] The magnetic interaction between unit cells in those NIMs was always neglected due to their very weak coupling. However, if these magnetic atoms are arranged close enough and their interaction cannot be neglected anymore, the coupling effect and the related dispersions are needed to pay much attention.

To this end, magnetic inductive waves[10,11] and magnetic plasmon propagations[12] were revealed in the one-dimensional SRR chains one after another in the past few years, as the magnetic coupling was considered. Moreover, magnetization waves were reported in this well recognized "fishnet structure" recently,[13] in which the authors observed the negative index mode exhibiting dispersions with respect to the in-plane wave vectors, though it is very weak (less than 0.08 eV within a $k_{\parallel} \sim 0.5\pi/a$). However, in a nearest work,[14] we have demonstrated a plasmonic property of the magnetic excitations in this fishnet structure, which results in not one but multiple magnetic modes associated with different in-plane wave vectors when they are coupled to corresponding incident light, referred as magnetic plasmon polaritons (MPPs). Actually, the well-informed negative index mode in previous reports[1–4,13] is the lowest MPP mode corresponding to the elementary reciprocal vector $G_{0,\pm 1}$ of the square lattice, and a higher MPP$(\pm 1, \pm 1)$ mode was elaborately elucidated in Ref. 14, indicating a plasmonic polariton similar to the surface plasmon polariton (SPP).[15,16] So, despite the lowest magnetic mode, dispersions of higher modes are highly expected.

In this paper, we focus our interest on the dispersions of the new-realized multiple MPP modes, especially the MPP$(\pm 1, \pm 1)$ one, and investigate their properties by analyzing the optical transmissions at oblique incidences in *s*- and *p*-polarization conditions. Since the visibility of MPP modes in the spectra is related with SPP enhanced transmissions,[14] a broader transmission band is needed in order to improve the identification of the dispersive MPP modes. A good method is to modify the primitive square holes to rectangular ones because the shape resonance coupled with SPP leads to a strong localized surface plasmon (LSP) excitation, resulting in a broad and redshifted transmission band (as $E\perp$ longer side).[17] In fact, recent reports exhibiting improved negative refraction properties are all based on this design.[2,3] In this way, we can conveniently adjust the structural parameter to accommodating the MPP's eigenfrequency to rightly locate inside the LSP transmission band, allowing for its observable frequency shifts.

[a)]Author to whom correspondence should be addressed.
[b)]Electronic mail: taoli@nju.edu.cn.
[c)]Electronic mail: zhusn@nju.edu.cn.

 

TABLE I. In-plane structural parameters for samples $A \sim E$.

| Sample | $P_x$ (nm) | $P_y$ (nm) | $a_x$ (nm) | $a_y$ (nm) |
|---|---|---|---|---|
| *A* | 600 | 600 | 300 | 300 |
| *B* | 600 | 600 | 430 | 300 |
| *C* | 710 | 600 | 430 | 300 |
| *D* | 800 | 600 | 430 | 300 |
| *E* | 500 | 500 | 430 | 300 |

## II. EXPERIMENTAL DETAILS

According to these considerations, we fabricate $Ag/SiO_2/Ag$ fishnet samples $A/B/C/D$ on quartz substrates with layer thickness of 35/40/35 nm and a sample *E* of 35/60/35 nm. Their in-plane structural parameters are listed in Table I. Here, $P_x$ ($P_y$) is the period of the hole lattice and $a_x$ ($a_y$) is the hole size in $x$ ($y$) direction, respectively. Experimentally, the primitive trilayer samples on quartz substrates are prepared by sputtering and followed with the focus ion beam (FIB) (FEI Company, 30 keV Ga ions) etching. These samples are all fabricated with $81 \times 81 = 6561$ units covering an area about $49 \times 49$ $\mu m^2$ for *A* and *B*, and a little larger or smaller for *C*–*E* due to their different periodicities. Figure 1(a) shows a typical FIB image of sample *B*. A *y*-polarized (*E* field along *y* direction) light (75 W, halogen lamp) is incident on the samples after a slight focalization, and transmissions are collected by an optical spectrum analyzer (ANDO, AQ-6315A) via a fiber coupler. Note that our samples are planted on a homemade rotational optical setup, which allows for the oblique incidence. The *s*- and *p*-polarization measurements are schematically shown in Fig. 1(b).

## III. RESULTS AND DISCUSSIONS

In Figs. 2(a) and 2(b), we demonstrate the measured and calculated transmission spectra of the samples $A/B/C/D$ at normal incidence, respectively. The numerical simulations

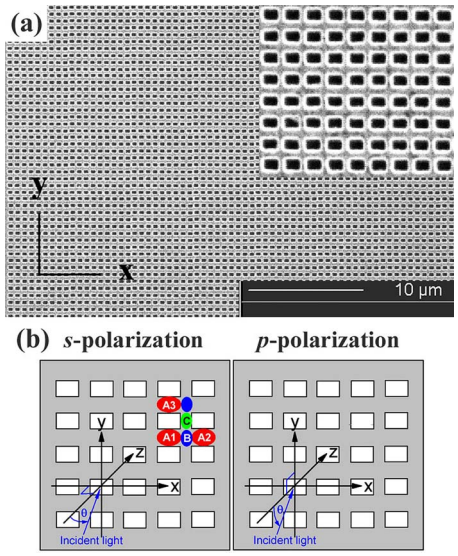


FIG. 1. (Color online) (a) Typical FIB image of sample *B*, whose in-plane period $P_x = P_y = 600$ nm and hole size $a_x = 430$ and $a_y = 300$ nm. (b) Schematics of the oblique incidences with an incident angle $\theta$ of *s*- and *p*-polarization cases. Color symbols marked with "A1," "A2," "A3," "B," and "C," schematically denote the "magnetic atoms."

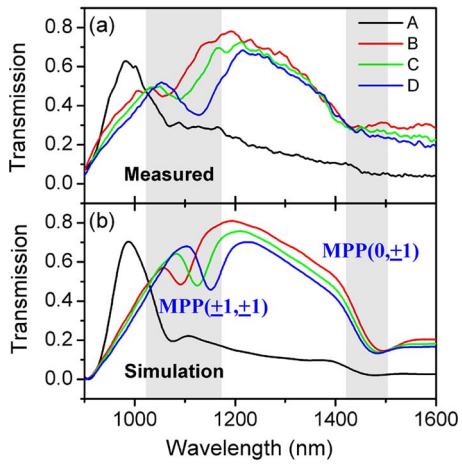


FIG. 2. (Color online) (a) Measured and (b) simulated transmission spectra of samples $A/B/C/D$ at normal incidence, in which two magnetic plasmon polariton modes are marked out.

are performed using a commercial software package (CST Microwave Studio) with Drude model for silver [$\omega_p = 1.37 \times 10^{16}$ $s^{-1}$, $\gamma = 8.5 \times 10^{13}$ $s^{-1}$ (Ref. 3)]. The overall agreements between experimental spectra and simulations are considerably good. All samples have inflexions at about 1430 nm in spectra, which are the lowest magnetic modes associated with elementary reciprocal vector $G_{0,1}$. At shorter wavelength, sample with square holes (*A*) has a narrow transmission peak, which is considered from the SPP excitation in the perforated metal surface.[14] However, samples with rectangular holes ($B/C/D$) exhibit stronger and broader redshifted transmission band due to excitations of LSP.[17] As expected, MPP($\pm 1, \pm 1$) mode (degenerated modes related with $G_{\pm 1,\pm 1}$) is well exhibited as a dip in the spectra, which appears more distinguishable as is adjusted into the center of the LSP transmission band (see sample *D*). Such a method of changing $P_x$ to modulate the MPP mode is well interpreted in Ref. 14. In the following, we will emphatically study the MPP dispersions with respect to the in-plane wave vectors $k_x$ and $k_y$.

First, oblique incidence of an *s*-polarized light with the incident angle $\theta$ is introduced by rotating the sample along *y* axis. Figures 3(a) and 3(b) display the transmission spectra with $\theta$ ranging from 0° to 22° of samples *C* and *D*, respectively. As we can see, the total profiles of broad LSP transmission band from 900 to 1400 nm are seldom changed as the incident angle is increased, while the MPP($\pm 1, \pm 1$) mode splits into two dips apparently. Expectedly, the mode shifts in sample *D* appear more evident than that in sample *C* due to its deeper involvement in the LSP band. In order to present more intuitive picture, the total transmissions of sample *D* are mapped in gray scale versus wave vector $k_x$ and wavelength λ in the *s*-polarization case, as shown in Fig. 4(a). Before looking into the details of MPP modes, we firstly inspect the dispersions of diffracted light on metal surfaces. According to Ebbesen's work,[16] we contribute the transmission minima to the Wood anomalous, which actually accord to the matching conditions for the reciprocal vectors to the wave vector of diffracted light. Its dispersion can be written as

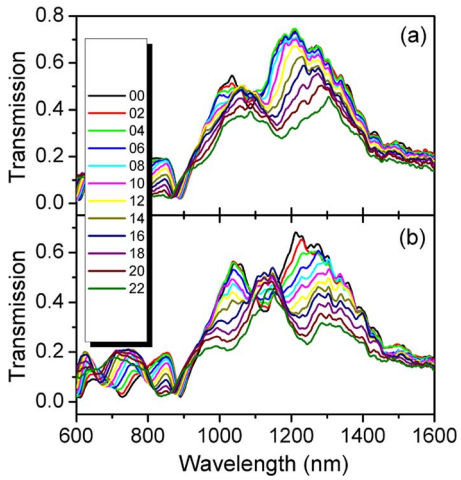


FIG. 3. (Color online) Measured transmission spectra of (a) sample *C* and (b) sample *D* with the incident angle ranging from 0° to 22° at *s*-polarization.

$$\lambda_{\text{wood}} = \frac{2\pi n_d}{|\mathbf{k} + \mathbf{G}_{m,n}|} = \frac{2\pi \cdot n_d}{|(k_x \pm mG_x)\hat{x} + (k_y \pm nG_y)\hat{y}|}. \quad (1)$$

Here, $n_d$ is the refractive index of dielectric medium; $G_x$ and $G_y$ are the elementary reciprocal vectors along $x$ and $y$ directions, respectively. We thus depict the dispersion curves (white dashed) in the $(\lambda, k_x)$ map marked by index $(m,n)$ and related media. Despite a little discrepancy, the tendencies of these dispersion curves fit the transmission minima relatively well.

Comparatively, we can write the MPP dispersion versus the in-plane wave vectors as

$$\lambda_{\text{MPP}(m,n)} = \frac{2\pi c}{|(k_x \pm mG_x)\hat{x} + (k_y \pm nG_y)\hat{y}|}\left(\frac{1}{\omega_{LC}}\right), \quad (2)$$

where $\omega_{LC}$ is the eigenfrequency of the *LC* resonance. With the simulated value of the eigenfrequency, we calculate the dispersion curves for each MPP mode. For *s*-polarization, as shown in Fig. 4(a) (black dashed curves), MPP$(0, \pm 1)$ keeps degenerated due to the absence of $G_x$, and slightly rises with

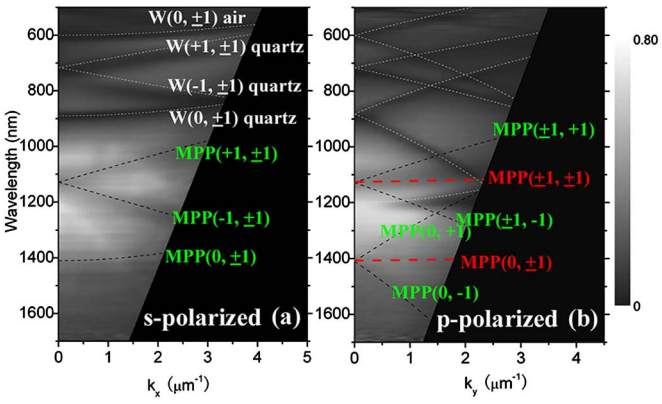


FIG. 4. (Color online) Measured transmission maps on an intuitive gray scale vs $\lambda$ and $k_x$ of sample *D* in (a) *s*-polarization and for (b) *p*-polarization. In the maps, white and black dashed curves correspond to the calculated dispersion line for diffracted light and MPP modes according to Eqs. (1) and (2), respectively; while the red dashed line is the calculated MPP modes by Eq. (3).

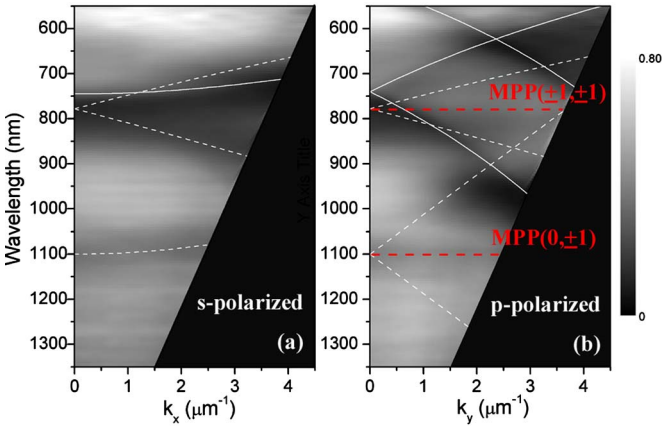


FIG. 5. (Color online) Measured transmission maps for sample *E* in (a) *s*-polarization and (b) *p*-polarization, in which solid curves are the dispersion of diffracted light and dashed curves are the calculated MPP modes by Eq. (2), and the red dashed line are calculated by Eq. (3).

increasing $k_x$; while MPP$(\pm 1, \pm 1)$ split into two branches $(+1, \pm 1)$ and $(-1, \pm 1)$, which are extremely coincident with two split darkness in transmission map. This good agreement convinces the plasmonic property of the proposed MPP model with analog property to the diffracted light or SPPs.[16]

Following the similar procedure, we analyzed the circumstance of the *p*-polarization of sample *D* by rotating the sample along $x$ axis ($E$ field still along $y$ direction), as the transmittances diagram versus the $\lambda$ and $k_y$ shown in Fig. 4(b). Firstly, we employ Eqs. (1) and (2) to calculate the dispersion curves of diffracted light and MPPs, respectively. It is seen that the dispersion curves of diffracted light and transmission minima are still in good coincidence, while the case for MPPs is quite different. According to Eq. (2), both modes $(0, \pm 1)$ and $(\pm 1, \pm 1)$ should split due to the breakup of degeneracy with the participation of $k_y$. However, they are still degenerate exhibiting a flat dispersive character in the transmission map. It is quite different from the diffracted light or SPP, which surely surprises us as well.

In order to make a confirmation on such phenomena of MPPs for two incidence conditions, we additionally inspect the sample *E*, whose lowest magnetic mode MPP$(0, \pm 1)$ was artificially adjusted rightly to inside the broad LSP band at normal incidence. The transmission maps of $(k_x, \lambda)$ and $(k_y, \lambda)$ for *s*- and *p*-polarizations are shown in Figs. 5(a) and 5(b), respectively, in which the calculated dispersions of the diffracted light (solid curves) and MPP modes (dashed curves) are displayed as well. Same to the former one, calculated results by Eq. (1) agree well with the measured one for the diffracted light for both cases, while those by Eq. (2) only fit MPPs in *s*-polarization. Nonsplit MPP modes with flat dispersions in *p*-polarization are exhibited again, obviously violating the calculated dispersion curves (white dashed), which is in good coincidence with the result of sample *D*.

In the following, we will get into the discussions about this particular dispersion of MPPs. The major difference between MPP and the diffracted light (or SPP) is that its plasmonic behavior comes from not the diffracted process but

the coupling of those separated magnetic atoms. Then let us look back into the schematics [Fig. 1(b)], when the magnetic modes excited by a *y*-polarized incidence, current loops along two-layered metallic segments form magnetic flux along *x* direction. Schematically, the flux generated from "magnetic atom A1" is remarkably interacted with "atom A2" via the bridge "atom B," resulting in a strong coupling. However, for A1 and A3, they are rather difficult to interact with each other due to the very weak magnetic induction. From this point, we find the clues for the anisotropic MPP dispersions. Since the in-plane wave vectors participating in the magnetic response rely on the coupling, the related wave vector would contribute little to the MPP modes if the magnetic atoms are weakly coupled in this direction. So, in *s*-polarization condition, strong coupling in *x* direction should split the $G_x$-related MPP mode, while the weak coupling in *y* direction causes $k_y$ can hardly affect all MPP modes at *p*-polarized incidence. For simplification, we may define that the magnetic atoms are coupled in *x* direction but not in *y* direction. Then, we can modify the dispersion of Eq. (2) as

$$\lambda_{\mathrm{MPP}(m,n)} = \frac{2\pi c}{|(\delta_y k_x \pm mG_x)\hat{x} + (\delta_x k_y \pm nG_y)\hat{y}|}\left(\frac{1}{\omega_{LC}}\right), \quad (3)$$

where $\delta_x$ and $\delta_y$ are introduced to describe the polarization. When the incident light is *x*-polarized (*y*-polarized), $\delta_x=1$ and $\delta_y=0$ ($\delta_y=1$ and $\delta_x=0$). With this modified formula, the dispersions of sample *D* and *E* at *p*-polarization appear as flat lines as the red dashed lines shown in Figs. 4(b) and 5(b) and actually agree well with the measured transmission maps.

## IV. CONCLUSION

In conclusion, we have studied the dispersion properties of MPP modes related with $G_{0,\pm1}$ and $G_{\pm1,\pm1}$ in trilayer fishnet structures in *s*- and *p*-polarization conditions. It is well demonstrated that at *s*-polarization the MPPs show analog dispersions to the diffracted light with corresponding $(m,n)$ ordered modes. Note that the mode $(\pm1,\pm1)$ exhibits stronger dispersive property than mode $(0,\pm1)$ does due to the evolvement of $k_x$ in this higher mode. However, in *p*-polarization case, the $k_y$ can hardly contribute to the MPPs resulting in very weak dispersive modes that remain degenerate. This phenomenon is explained by different coupling property of magnetic atoms in *x* and *y* directions as are related with *y*-polarized light. Our finding provides a good cognition on the new-realized MPP modes in fishnet structure, which is expected to be useful in the metamagnetism designs or other optical metamaterial explorations.

## ACKNOWLEDGMENTS

This work is supported by the National Natural Science Foundations of China (Grant Nos. 10704036, 10604029, 10534020), and by the State Key Program for Basic Research of China under Grant No. 2006CB921804.

[1] S. Zhang, W. Fan, N. C. Panoiu, K. J. Malloy, R. M. Osgood, and S. R. J. Brueck, Phys. Rev. Lett. **95**, 137404 (2005).
[2] G. Dolling, C. Enkrich, M. Wegener, C. M. Soukoulis, and S. Linden, Science **312**, 892 (2006).
[3] G. Dolling, C. Enkrich, M. Wegener, C. M. Soukoulis, and S. Linden, Opt. Lett. **31**, 1800 (2006).
[4] G. Dolling, M. Wegener, C. M. Soukoulis, and S. Linden, Opt. Lett. **32**, 53 (2007).
[5] J. B. Pendry, A. J. Holden, D. J. Robbins, and W. J. Stewart, IEEE Trans. Microwave Theory Tech. **47**, 2075 (1999).
[6] R. A. Shelby, D. R. Smith, and S. Schultz, Science **292**, 77 (2001).
[7] D. R. Smith, J. B. Pendry, and M. C. K. Wiltshire, Science **305**, 788 (2004).
[8] V. M. Shalaev, Nat. Photonics **1**, 41 (2007).
[9] C. M. Soukoulis, S. Linden, and M. Wegener, Science **315**, 47 (2007).
[10] E. Shamonina, V. A. Kalinin, K. H. Ringhofer, and L. Solymar, J. Appl. Phys. **92**, 6252 (2002).
[11] O. Sydoruk, O. Zhuromskyy, E. Shamonina, and L. Solymar, Appl. Phys. Lett. **87**, 072501 (2005).
[12] H. Liu, D. A. Genov, D. M. Wu, Y. M. Liu, J. M. Steele, C. Sun, S. N. Zhu, and X. Zhang, Phys. Rev. Lett. **97**, 243902 (2006).
[13] G. Dolling, M. Wegener, A. Schadle, S. Burger, and S. Linden, Appl. Phys. Lett. **89**, 231118 (2006).
[14] T. Li, J. Q. Li, F. M. Wang, Q. J. Wang, H. Liu, S. N. Zhu, and Y. Y. Zhu, Appl. Phys. Lett. **90**, 251112 (2007).
[15] T. W. Ebbesen, H. J. Lezec, H. F. Ghaemi, T. Thio, and P. A. Wolff, Nature (London) **391**, 667 (1998).
[16] H. F. Ghaemi, T. Thio, D. E. Grupp, T. W. Ebbesen, and H. J. Lezec, Phys. Rev. B **58**, 6779 (1998).
[17] K. J. K. Koerkamp, S. Enoch, F. B. Segerink, N. F. van Hulst, and L. Kuipers, Phys. Rev. Lett. **92**, 183901 (2004).